Resistivity anisotropy of $A\mathrm{Fe_2As_2}$ (A=Ca, Sr, Ba): Direct versus Montgomery technique measurements

M. A. Tanatar,[1,*] N. Ni,[1,2] G. D. Samolyuk,[1,†] S. L. Bud'ko,[1,2] P. C. Canfield,[1,2] and R. Prozorov[1,2,‡]
[1]*Ames Laboratory, Ames, Iowa 50011, USA*
[2]*Department of Physics and Astronomy, Iowa State University, Ames, Iowa 50011, USA*
(Received 4 March 2009; published 29 April 2009)

The anisotropy of electrical resistivity was measured in parent compounds of the iron-arsenic high-temperature superconductors $A\mathrm{Fe_2As_2}$ with alkali earth elements A=Ca, Sr, and Ba. Measurements were performed using both the Montgomery technique and direct resistivity measurements on samples cut along principal crystallographic directions. The anisotropy ratio $\gamma_\rho=\rho_c/\rho_a$ is well below ten for all compounds in the whole temperature range studied (4–300 K), in notable contrast to previous reports. The anisotropy at room temperature increases from about two in Ca to about four in Sr and Ba. In all compounds the resistivity ratio decreases on cooling through the structural/antiferromagnetic transition temperature T_{SM}, with the change mainly coming from stronger variation in ρ_a as compared with ρ_c. This suggests that the transition affects stronger the two-dimensional parts of the Fermi surface. We compare our experimental observations with band-structure calculations, and find similar trend in the evolution of anisotropy with the size of A ion. Our results show that the electronic structure of the iron pnictides has large contribution from three-dimensional areas of the Fermi surface.

DOI: 10.1103/PhysRevB.79.134528 PACS number(s): 74.70.Dd, 72.15.−v, 74.25.Jb

I. INTRODUCTION

Following the original ideas by Little[1] and Ginzburg,[2] it was generally accepted that low dimensionality of the electronic spectrum is an important prerequisite for finding superconductivity with high transition temperatures. These ideas fueled study of superconductivity in chained and layered materials,[3] including transition-metal chalcogenides,[4] organics,[5] and most recently cuprates,[6] MgB_2 (Ref. 7) and Sr_2RuO_4.[8] Discovery of the iron-arsenide superconductors,[9,10] characterized by layered structure of Fe-As layers sandwiched between the layers of different chemical composition, seem to suggest that electronic structure of these materials may be two dimensional as well. The $3d$ electronic orbitals of iron make the main contribution to the electronic bands close to the Fermi energy in iron arsenides, and thus high anisotropy is naturally expected. This was suggested by early band-structure calculations,[11] and seemed to find support in high ratio of electrical resistivity when measured for current flowing perpendicular to the Fe-As plane (ρ_c) and along it (ρ_a), $\gamma_\rho \equiv \rho_c/\rho_a \sim 100$, as reported for the nonsuperconducting parent compounds $BaFe_2As_2$ (Ref. 12) and $SrFe_2As_2$,[13] as well as for superconducting Co-doped $BaFe_2As_2$.[14] Following this suggestion, formation of an antiferromagnetic state in the parent compounds below a temperature T_{SM} of simultaneous structural/magnetic transition (in the range from 137 K in A=Ba to 210 K in A=Sr) was assigned to the development of the spin density wave, gapping part of the Fermi surface due to nesting.

Recently, however, we found[15] notably smaller anisotropy of the electrical resistivity, γ_ρ, of the superconducting upper critical fields, $\gamma_H \equiv \frac{H_{c2ab}}{H_{c2c}}$,[16] of the London penetration depth $\gamma_\lambda \equiv \frac{\lambda_c}{\lambda_{ab}}$ and of the superconducting critical current $\gamma_j \equiv \frac{j_{ca}}{j_{cc}}$ in the optimally Co-doped $Ba(Fe_{0.926}Co_{0.074})_2As_2$, $T_c \approx 23$ K. Moreover, the anisotropies had values very close to the theoretically expected relations between these quantities, $\gamma_H = \gamma_\lambda = \sqrt{\gamma_\rho}$.[15]

Since anisotropy is an important parameter, both for the mechanism of the magnetic state formation in the parent compounds and for superconductivity in the doped iron arsenides, we have undertaken comprehensive characterization of the resistivity anisotropy in the parent compounds of $A\mathrm{Fe_2As_2}$. Our main finding is that anisotropy is generally very low, inconsistent with two-dimensional (2D) models of the electronic structure.

II. EXPERIMENT

Single crystals of $BaFe_2As_2$ and of $SrFe_2As_2$ were grown from FeAs flux from a starting load of metallic Ba(Sr) and FeAs, as described in detail elsewhere.[16] Crystals were thick platelets with sizes as big as $12\times8\times1$ mm^3 and large faces corresponding to the tetragonal (001) plane. Single crystals of $CaFe_2As_2$ were grown from Sn flux, as described by Ni *et al.*[17] The crystal quality of all samples was confirmed with x-ray Laue measurements on single crystals, which found resolution limited narrow peaks, see Refs. 16 and 17 for details. No traces of either FeAs flux (by single-crystal x-ray) or Sn flux (with wavelength dispersive electron probe microanalysis) were found.

In our study of resistivity anisotropy in optimally doped superconducting $Ba(Fe_{1-x}Co_x)_2As_2$ with x=0.074, we have found that exfoliation of samples dramatically alters the sample resistivity, especially for measurements in configurations with current along tetragonal c axis.[15] Due to the softness of the materials, their cutting and shaping into transport samples inevitably introduces cracks, which affect the effective geometric factors of the sample. A strong tendency to exfoliate prevents the cutting of samples with $c \gg a$. Partial cleaving by exfoliation is one of the most likely reasons for

the unusually high anisotropy, as found in previous studies.[12–14]

Samples for electrical resistivity measurements with current flow along the [100] a axis in the tetragonal plane (ρ_a) were cut into bars of $(2-3)\times(0.1-0.2)\times(0.1-0.2)$ mm^3 ($a\times b\times c$). Samples for electrical resistivity measurements with current flow along the tetragonal c axis (ρ_c) were cut into $(0.3-0.7)\times(0.3-0.7)\times(0.1-0.5)$mm^3 ($a\times b\times c$) bars. All sample dimensions were measured with an accuracy of about 10%. Contacts to the samples were made by attaching silver wires with a silver alloy, resulting in an ultralow contact resistance (less than 100 $\mu\Omega$). Measurements of ρ_a were made in both standard four-probe and two-probe configurations, and gave identical results, see Ref. 18. Measurements of ρ_c were made in the two-probe sample configuration. Contacts were covering the whole ab plane area of the c-axis samples. A four-probe scheme was used to measure the resistance down to the contact to the sample, i.e., the sum of the actual sample resistance R_s and contact resistance R_c was measured. Taking into account that $R_s \gg R_c$, this represents a minor correction of the order of 1–5 %. This can be directly seen for superconducting samples[15] at temperatures $T<T_c$, where $R_s=0$ and the measured resistance represents R_c.

Samples for Montgomery technique measurements of the resistivity anisotropy ratio, γ_ρ, were typically of the same size as samples for ρ_c measurements. They had a ratio of sample dimensions along a, l_a, and along c, l_c, between two and three. For resistivity anisotropy measurements in the ac plane, contacts were made over whole lengths of the four sample edges along b direction, with length l_b. A projection of the contacts on the ac plane is schematically shown in inset of Fig. 3 (below). Four-probe resistivity measurements were made by sending current I_1 along one side of the sample (between contacts 1–4 for current along a) and measuring voltage V_1 on the opposite side (between contacts 2 and 3). Thus we determined the resistance $R_1=V_1/I_1$. In a next step the direction of the current was rotated by 90°, with I_2 flowing along c axis between contacts 1 and 2, and voltage V_2 measured between contacts 3 and 4. The ratio was used to define $R_2=V_2/I_2$. The ratio of the measured resistances, R_1/R_2, was used to determine the ratio of effective sample dimensions, l'_a/l'_c, using calculations of Ref. 20. A comparison of the actual (l_a/l_c) and the effective (l'_a/l'_c) sample dimensions was used to determine the resistivity anisotropy as $(\rho_2/\rho_1)^{1/2}=(l'_c/l'_a)/(l_c/l_a)$.[19] Since the whole idea of the Montgomery technique is based on a homogeneous current distribution in the sample, the structural integrity of the sample, as well as the lack of inclusions of foreign materials (flux and solder) and voids play crucial role in measurements of this type.

Because the contacts to the samples were extended over the whole length along l_b we used a thin slab approximation[19] in the data analysis. During analysis we assumed the precise position of the contacts at the corners of the sample and neglected their size in the basal ac plane of the rectangular prism. Since (1) the actual size of the contacts is 10–20 % of the sample dimensions and is not negligible as compared to either l_a or l_c, (2) the contact positions and shape can deviate from ideal, and (3) the sample section in the ac plane is often not ideal and deviates from the assumed perfect rectangular, these factors bring sizable errors into the estimated anisotropy. To make our best effort, we were reproducing the results of Montgomery resistivity anisotropy measurements on several samples of each compound. We estimate the systematic error of these measurements as on the order of ±50% for the anisotropy ratio.

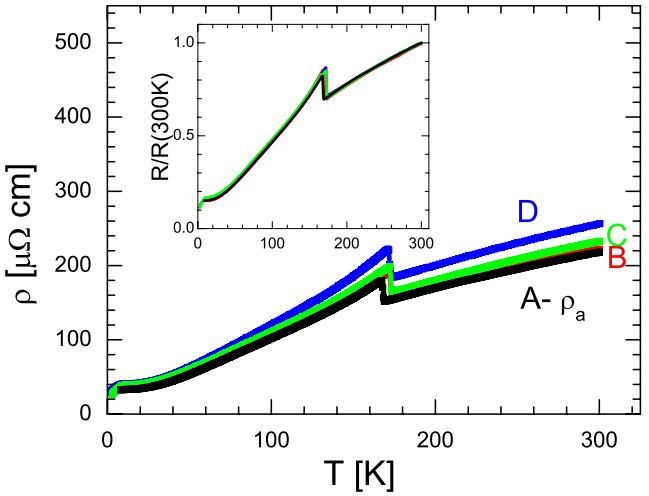

FIG. 1. (Color online) Temperature dependence of ρ_a measured on four different samples of $CeFe_2As_2$ (main panel). The inset shows the same data normalized to a value at 300 K. Samples are labeled A–D in line with increase in the room-temperature resistivity value.

Band-structure calculations were performed using the full potential linearized augmented plane-wave (FLAPW) approach[21] and the local-density approximation (LDA).[22] The mesh of $31\times31\times31$ $\vec{k}$ points was used for the Brillouin-zone integration. We have used experimental lattice constants for the $BaFe_2As_2$ (Ref. 23), $SrFe_2As_2$ (Ref. 24), and $CaFe_2As_2$ (Ref. 25). The Fermi velocities were calculated using the BOLZ-TRAP package.[26]

III. RESULTS

A. $CaFe_2As_2$

In Figs. 1 and 2 we show the temperature dependence of the electrical resistivities ρ_a and ρ_c (main panels in the figures), and the same data normalized by room-temperature values (insets). The data with current along the plane was taken for four samples while the data for interplane current was taken for three samples. The shape of the temperature-dependent resistivity is very well reproduced between the samples of the same sort. Moreover, the value of the in-plane resistivity is very well reproduced as well, with the value at room temperature 232 ± 15 $\mu\Omega$ cm staying within the uncertainty of the geometric factor determination. The value of the interplane resistivity is more spread, from 456 $\mu\Omega$ cm for sample A to 1365 $\mu\Omega$ cm for sample C. Average over three samples gives a value of 800 ± 400 $\mu\Omega$ cm. As we have shown in our previous report on the superconducting samples,[15] the lowest values are the most reliable since the effect of exfoliations tends to increase ρ_c. This finds direct support in case of parent compounds, as shown by the com-

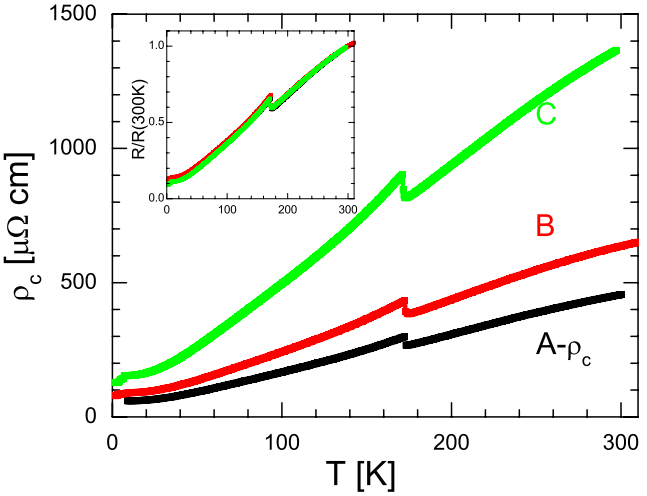

FIG. 2. (Color online) Temperature dependence of ρ_c measured on three samples of $CaFe_2As_2$ (main panel). The inset shows the same data normalized by the value of ρ_c at 300 K. The curves are labeled alphabetically in line with room-temperature resistivity increase.

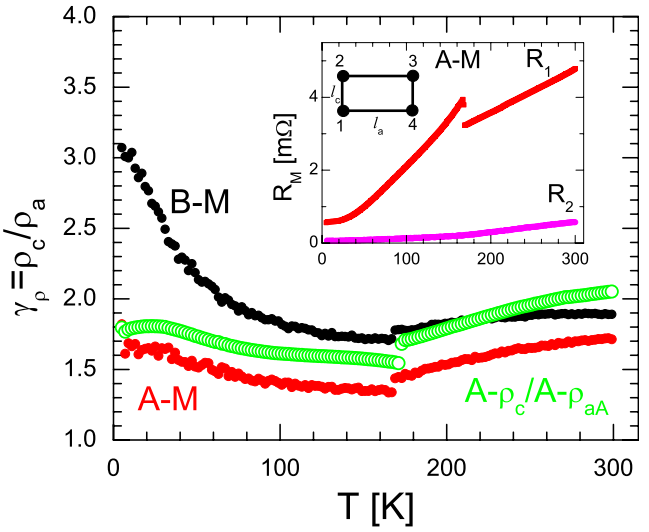

FIG. 3. (Color online) Temperature dependence of the ratio of resistivities $\gamma_\rho \equiv \rho_c/\rho_a$ as determined from the Montgomery technique (solid symbols), and from the ratio of independently measured ρ_a and ρ_c for samples with the lowest resistivities, A-ρ_c and A-ρ_a (open symbols). The inset shows raw R_1 and R_2 data for sample A-M, and schematics of contact configuration during anisotropy measurements using Montgomery technique. Sample has rectangular cross section in the ac plane with dimensions l_1 (along a) and l_2 (along c). Contacts are located at the corners of the rectangle and run in the direction perpendicular to the plane of the figure along l_3 (parallel b). Two sets of four-probe resistivity measurements are performed: in the first run current I_1 is flowing between contacts 1 and 4 along l_1 while voltage V_1 is measured between contacts 2 and 3, their ratio determines resistance $R_1 = V_1/I_1$; in the second run direction of the current I_2 is along l_2 between contacts 1 and 2 while voltage V_2 is measured between contacts 3 and 4, and $R_2 = V_2/I_2$. The anisotropy γ_ρ is calculated using R_2/R_1 and l_2/l_1 ratios as discussed in Refs. 19 and 20.

parison with Montgomery technique measurements, Fig. 3. The inset shows the temperature dependence of the raw data, R_1 and R_2, for sample A with Montgomery contact configuration while main panel shows comparison of the $\gamma_\rho = \rho_c/\rho_a$ ratio as determined for two samples in Montgomery configuration, and from direct ρ_a and ρ_c measurements for samples A (lowest resistivity) with in-plane and interplane currents. There is semiquantitative agreement between γ_ρ at room temperature determined in these two very different ways, with $\gamma_\rho = 1.7$ for sample A-M, 1.9 for sample B-M, and 2.1 from the comparison of direct resistivity measurements using the data for the lowest resistivity for ρ_c. Comparison of the average ρ_a and ρ_c values gives a ratio of about four, notably larger than that found in Montgomery technique measurements.

It should be pointed out that good correspondence between the temperature-dependent anisotropy ratio as determined from three different measurements is a very strong argument for the correct anisotropy determination. As can be seen from comparison of insets of Figs. 1 and 3, R_1 and ρ_a reveal quite different temperature dependences, despite the fact that both are using in-plane current. This difference is even more striking when comparing measurements with interplane current flow, R_2 and ρ_c (insets of Figs. 2 and 3): while the former does not show even a trace of resistance increase at T_{SM}, the latter reveals it clearly.

The ratio, as determined from independent measurements of ρ_a and ρ_c, can be affected by the difference in sample quality and in a pattern of structural domains. Sample resistivity can be written as $\rho = \rho_0 + \rho_{in}$ and the residual resistivity ρ_0 can vary from sample to sample. This difference in ρ_0 is actually revealed by the comparison of the normalized curves in the insets of Figs. 1 and 2. Therefore, the behavior of the temperature-dependent anisotropy reflects the intrinsic properties the best at high temperatures. Montgomery technique measurements are performed on one sample and therefore they are affected to a lesser extent by this difference. Based on these considerations we conclude that measurements on sample A-M, characterized by the smallest difference of R_1 and R_2, are most representative for intrinsic temperature-dependent anisotropy.

Of note is the temperature dependence of ρ_a and ρ_c. Previous measurements found identical $\rho_a(T)$ curve with notable increase in resistivity below the structural/antiferromagnetic transition at 173 K.[17] This decrease reflects presumably partial loss of the density of states (DOS). The transition shows a hysteresis of about 2 K. The temperature dependence of ρ_c is similar; however, here the increase in resistivity below the transition is notably smaller. As a result, the resistivity anisotropy decreases below the transition. On further cooling, the anisotropy continues to increase but only slightly.

B. $SrFe_2As_2$

In Figs. 4 and 5 we show the temperature dependence of the electrical resistivities ρ_a and ρ_c (main panels in the figures), and the same data normalized by the room-temperature values (insets of the figures) for $SrFe_2As_2$. The data with current along the plane was taken for four samples while the data for interplane current was taken for five samples.

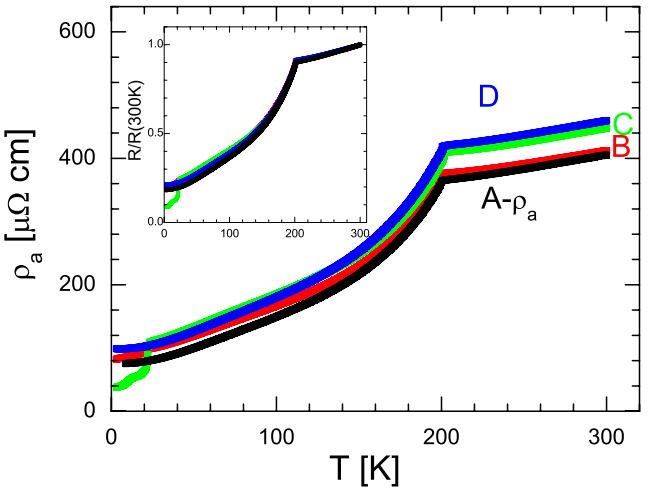

FIG. 4. (Color online) Temperature dependence of ρ_a measured on four different samples of $SrFe_2As_2$ (main panel). The inset shows the same data normalized to a value at 300 K. Samples are labeled A–D in line with increase in the room-temperature resistivity value.

The value of the in-plane resistivity is well reproduced within error bars of geometric factor determination; at room temperature it is 430 ± 24 $\mu\Omega$ cm. The shape of the temperature-dependent resistivity, $\rho_a(T)$, is well reproduced as well, see inset of Fig. 4. On cooling ρ_a gradually decreases, the rate of decrease increases below $T_{SM}=205$ K. A close inspection of the data reveals a tiny increase in the very vicinity of the transition (hard to see in Fig. 4).

The value of the interplane resistivity is more spread, from 1790 $\mu\Omega$ cm for sample A to 3960 $\mu\Omega$ cm for sample E. Note that samples with higher resistivity show notably different temperature dependence (inset of Fig. 5). In addition, they clearly show traces of superconductivity. Since superconductivity in pure $SrFe_2As_2$ is induced by residual strain,[27] as well as by hydrostatic pressure,[28] this allows us to link the abnormally high-resistivity values with the presence of deformed areas in the samples. This agrees well with the conclusion of our previous study, linking high-resistivity values with partial exfoliation,[15] in which case strained regions are easily formed, as well as with small volume fraction of superconducting inclusions found in magnetization studies.[27] The temperature dependence of interplane resistivity, $\rho_c(T)$, shows the same features as $\rho_a(T)$; however, a flattening above T_{SM} and the decrease below T_{SM} are more pronounced in ρ_c.

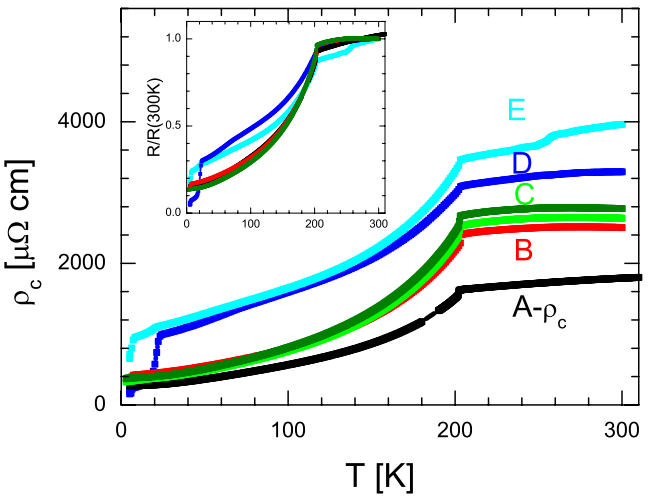

FIG. 5. (Color online) Temperature dependence of ρ_c measured on five samples of $SrFe_2As_2$ (main panel). Sample C was measured twice to check the effect of thermal cycling on resistivity value, the lower curve represents initial run. The inset shows the same data normalized by the value of ρ_c at 300 K. The curves are labeled alphabetically in line with room-temperature resistivity increase.

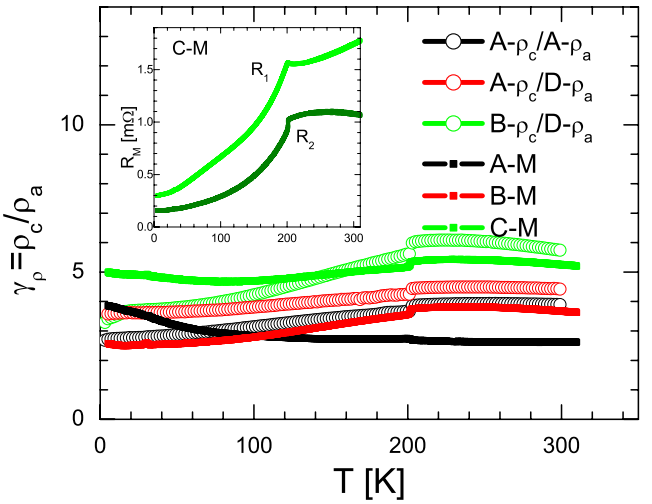

FIG. 6. (Color online) Temperature dependence of the ratio of resistivities $\gamma_\rho \equiv \rho_c/\rho_a$ as determined from the Montgomery technique (solid symbols), and from the ratio of independently measured ρ_a and ρ_c for several different samples (open symbols). The inset shows raw R_1 and R_2 data for sample C-M measured in Montgomery configuration.

The γ_ρ anisotropy ratio in $SrFe_2As_2$, as determined from direct measurements and from Montgomery technique measurements, is plotted in Fig. 6. Larger open symbols show the temperature dependence of the γ_ρ ratio of resistivities for selected samples: samples with lowest measured resistivities at room temperature, A-ρ_c/A-ρ_a, sample with lowest ρ_c with sample with highest ρ_a, A-ρ_c/D-ρ_a, as well as ratio of second highest resistivity sample B for interplane resistivity and highest resistivity sample D for in-plane resistivity, B-ρ_c/D-ρ_a. Small solid symbols show γ_ρ as calculated following Montgomery technique procedure based on the R_1 and R_2 raw data (shown for sample C in inset of Fig. 6). There is very good general agreement between the two measurements. Note that the ratio of the lowest ρ_c and ρ_a reproduces well the temperature dependence as well as magnitude of the γ_ρ for two samples measured in Montgomery technique. The most characteristic features of this behavior are slight increase in the anisotropy on approaching the structural/magnetic transition from above, sharp drop of the anisotropy at the transition, and small γ_ρ decrease on further cooling.

Of note, neither the value of the anisotropy nor the temperature dependence of interplane resistivity, $\rho_c(T)$, are consistent with findings of the previous study.[13] The difference

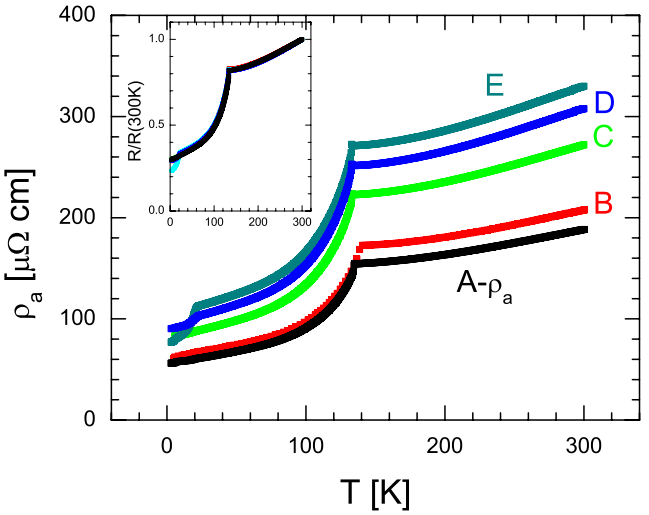

FIG. 7. (Color online) Temperature dependence of ρ_a measured on five different samples of $BaFe_2As_2$ (main panel). The inset shows the same data normalized to the resistivity values at 300 K. Samples are labeled A–E in line with increase in the room-temperature resistivity.

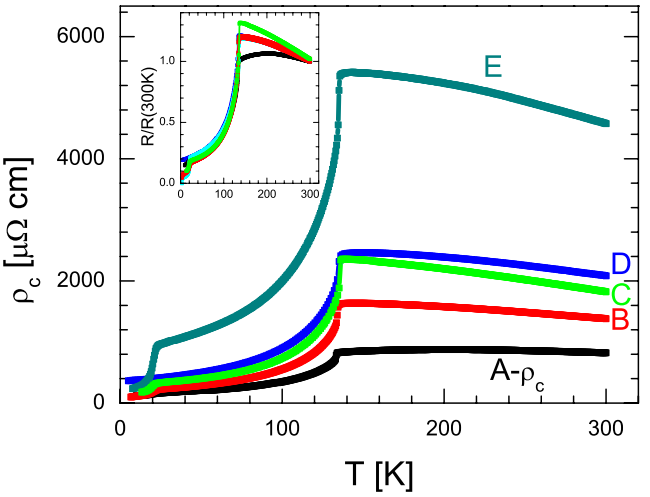

FIG. 8. (Color online) Temperature dependence of ρ_c measured on five samples of $BaFe_2As_2$ (main panel). The inset shows the same data normalized by the values of ρ_c at 300 K. The curves are labeled alphabetically in line with room-temperature resistivity increase.

of magnitude is dramatic, with anisotropy in the range of three to five in our case as compared with 130 in the previous study. Since no detail of the measurement procedure or its reproducibility, sample to sample, is given in Ref. 13, we cannot comment on the nature of the difference. We speculate that heavy contamination of the measured ρ_c data with ρ_a and strong deviations of the current path from the projected one must be the reason for the incorrect anisotropy determination in a previous study.

C. $BaFe_2As_2$

In Figs. 7 and 8 we show the temperature dependence of the electrical resistivities ρ_a and ρ_c (main panels in the figures), and the same data normalized by room-temperature values (insets of the figures) for $BaFe_2As_2$. The data for both current directions were taken for sets of five samples each.

The value of the in-plane resistivity in $BaFe_2As_2$ is the most scattered among the three compounds. The spread notably exceeds the error bars of geometric factor determination, giving the value at room temperature of 260 ± 55 $\mu\Omega$ cm. The shape of the resistivity temperature dependence $\rho_a(T)$ is reproduced well, with the only exception for the presence of partial superconducting transition in the samples D and E with the highest resistivity. This again suggests that these samples have strained regions, relating them with partial cracks. On cooling ρ_a gradually decreases, with the decrease rate being enhanced below $T_{SM}=137$ K.

The value of the interplane resistivity is even more spread, from 910 $\mu\Omega$ cm for sample A to 4540 $\mu\Omega$ cm for sample E. Note that, similar to $SrFe_2As_2$, the samples with higher resistivity show more pronounced superconducting feature, suggesting the existence of areas with high internal pressure. The value over five samples averages to 1760 ± 1310 $\mu\Omega$ cm; when excluding from consideration the outstanding sample E, averaging gives 1490 ± 390 $\mu\Omega$ cm. The shape of the temperature-dependent resistivity (inset of Fig. 5) is not reproduced as good as that for Ca and Sr compounds. Its pronounced feature is the increase in ρ_c on cooling down from room temperature. For four samples the increase continues all the way down to T_{SM}, followed by a decrease typical of a metal below. In one of the samples, [A-$\rho_c(T)$ curve in Fig. 8], the $\rho_c(T)$ shows a broad maximum at around 200 K and practically flattens below in the range down to T_{SM}.

The γ_ρ anisotropy ratio in $BaFe_2As_2$, as determined from direct measurements and from Montgomery technique measurements, are plotted in Fig. 9. The larger open symbols show the temperature dependence of the γ_ρ ratio of resistivities for selected samples: samples with lowest measured resistivities at room temperature, A-ρ_c/A-ρ_a, sample with lowest ρ_c with sample with medium ρ_a, A-ρ_c/C-ρ_a, as well as ratio of the medium resistivity sample C for interplane resistivity and medium resistivity sample C for in-plane resistivity, C-ρ_c/C-ρ_a. Small solid symbols show γ_ρ calculated following Montgomery technique procedure, using R_1 and R_2 raw data shown for sample A-M in inset of Fig. 9. The two ways of resistivity anisotropy determination agree in general, the agreement being the best when comparing the ratios obtained for lowest ρ_c. Anisotropy at room temperature is between three and five, similar to $SrFe_2As_2$. The spread of the ratios is bigger due to bigger scatter in the resistivity value both for ρ_a and ρ_c.

The most characteristic features of the temperature dependence of γ_ρ in $BaFe_2As_2$ are: increase in anisotropy on cooling down to T_{SM}, sharp drop at the transition, and slow decrease in the anisotropy below the transition.

IV. DISCUSSION

A. Resistivity anisotropy versus size of *A* element

The comparison of the Montgomery and direct resistivity anisotropies for the three different AFe_2As_2 compounds sug-

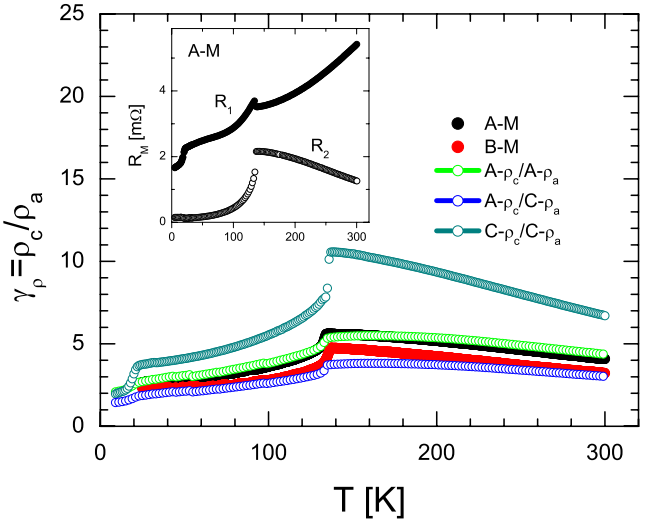

FIG. 9. (Color online) Temperature dependence of the ratio of resistivities $\gamma_\rho \equiv \rho_c/\rho_a$ as determined from the Montgomery technique (solid symbols), and from the ratio of independently measured ρ_a and ρ_c for some representative samples (open symbols). The inset shows raw R_1 and R_2 data for sample C-M measured in Montgomery configuration.

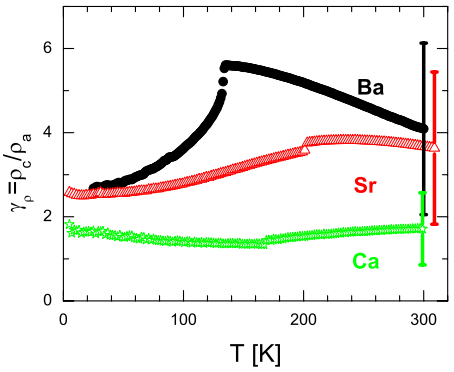

FIG. 10. (Color online) Temperature dependence of the anisotropy ratio $\gamma_\rho = \rho_c/\rho_a$ for $CaFe_2As_2$, $SrFe_2As_2$, and $BaFe_2As_2$. The error bars represent the evaluated systematic error of the anisotropy determination.

gests that the best agreement between the two types of anisotropy determinations is obtained when using samples with the lowest ratio of R_1 and R_2 resistances in the Montgomery measurements, and the lowest resistivity value for ρ_c. This is consistent with the conclusion of our previous study[15] on resistivity anisotropy in the superconducting $BaFe_2As_2$ doped with Co. We now turn to comparison of the data for different compounds using these criteria for selection.

In Fig. 10 we compare the temperature-dependent anisotropy ratios for the three AFe_2As_2 compounds. Despite sizable systematic error, comparison reveals a clear trend in the evolution of $\gamma_\rho(T)$. First, at room temperature the ratio is the lowest in the Ca compound ($\sim$2) while the anisotropy ratios of the Sr and Ba compounds (about four) are the same within error bars. Both these numbers are too low to be discussed in the two-dimensional Fermi-surface scenario.

The temperature-dependent anisotropy reveals systematic evolution with the size of the A atom as well. In the Ca compound γ_ρ decreases on cooling from room temperature down to T_{SM}, shows a down jump at T_{SM}, and slightly increases below. In the Sr compound the anisotropy very slightly increases down to T_{SM}, jumps down at the transition, and gradually decreases on further cooling. In the Ba compound the anisotropy increases gradually all the way down to T_{SM}, below which the anisotropy goes down very rapidly. Even though the γ_ρ ratios for the Sr and Ba compounds are very close both at room temperature and at low temperatures, the anisotropy of the Ba compound becomes more pronounced in the intermediate temperature range, especially above T_{SM}. Thus we conclude that the anisotropy follows the ionic radius of alkali earth elements, similar to the predictions of the band-structure calculations.

B. Band structure

A key structural feature of the iron-arsenide compounds, which makes a profound effect on their electronic structure, is the location of the As atoms above and below the layer of Fe atoms. The band dispersion along the tetragonal c direction is mainly determined by the overlap of As orbitals. Thus the anisotropy of the electronic structure is extremely sensitive to the displacement coordinate Z_{As} of As atom in the unit cell with respect to the Fe layers.

Since the actual location of the As atoms can vary, in our calculations in the paramagnetic phase of $BaFe_2As_2$, we have used two positions. In the first case, the position of As atoms was determined from the calculated minima of the total energy. We refer to this as the calculated or relaxed position below. The position of the As atom, $Z_{As}=0.341$, as determined in our analysis, is very close to the positions found in previous calculations, $Z_{As}=0.342$ (Ref. 29) but is signifi-

TABLE I. Calculated kinetic characteristics of AFe_2As_2 compounds in nonmagnetic states.

	σ_{xx}/τ	σ_{zz}/τ	σ_{xx}/σ_{zz}	DOS	Vol.	v_x	v_z	Z_{As}	Reference
Compound/Units	$10^{19}/(\Omega\ \mathrm{m\ s})$	$10^{19}/(\Omega\ \mathrm{m\ s})$		1/(eV f.u.)	Å^3	10^5 m/s	10^5 m/s		
$CaFe_2As_2$ collapsed	15.1	23.6	0.64	4.5	566.02	1.33	1.667	0.366	25
$CaFe_2As_2$	18.7	12.5	1.5	6.8	602.45	1.24	1.01	0.372	25
$SrFe_2As_2$	16.0	2.2	7.2	5.0	642.93	1.380	0.515	0.360	24
$BaFe_2As_2$	14.0	1.1	12.1	4.7	690.31	1.380	0.398	0.355	23
$BaFe_2As_2$	14.4	6.13	2.35	3.0	690.31	1.75	1.14	0.341	calculated

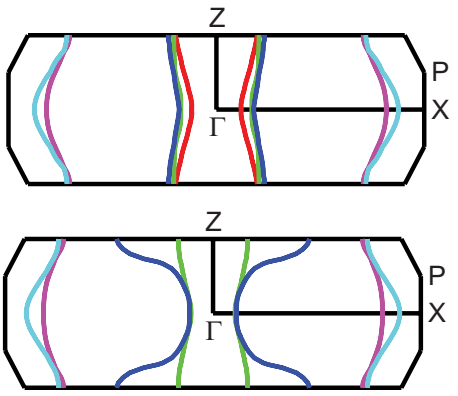

FIG. 11. (Color online) Cross section of the Fermi surface of $BaFe_2As_2$ by the ΓXZ plane in the Brillouin zone. The position of the As atom in the lattice, Z_{As}, was assumed corresponding to experimentally measured (Ref. 23) (top panel) or to the minimum of the total crystal energy (bottom panel). Variation in Z_{As} affects most strongly the sheets of the Fermi surface surrounding the Γ point in the Brillouin zone.

cantly lower than the experimental value of Z_{As}=0.355 at room temperature.[23] The Fermi velocities, calculated using the BOLZ-TRAP[26] package, are very sensitive to the As positions as well. A similar trend is found in magnetic properties.[29,30] The downshift by 0.16 Å increases both the band dispersion and the Fermi velocity along the z direction. The calculations with relaxed Z_{As} give V_{Fa}^2/V_{Fc}^2=3 for pure $BaFe_2As_2$; with the experimental Z_{As} we come to much larger anisotropy of 12.1. These two anisotropy values should be compared with the anisotropy of about four, as found for this compound in our experiment. The resistivity anisotropies using experimental Z_{As} for all compounds follow ionic radius of alkali earth elements, similar to a trend found in the experiment. We summarize the calculated anisotropies in Table I.

The calculation shows that the anisotropy of the Fermi velocities, averaged over the Fermi-surface sheets, varies a lot with Z_{As}. However, when looking at individual Fermi-surface sheets, a notable difference in response to variation in Z_{As} is found (Fig. 11). The shape of the central sheet of the Fermi surface, surrounding the Γ point of the Brillouin zone, is most sensitive to the position of the arsenic atom, and for relaxed Z_{As} it develops pronounced warping. Other sheets remain cylindrical, and therefore most correct description of the electronic structure should be as a combination of two-dimensional and three-dimensional (3D) portions. In this case contribution of the three-dimensional central sheet to ρ_c would shunt more anisotropic contributions of the rest of the Fermi surface.

Obviously, our experimental values of the anisotropy are compatible with both anisotropic three-dimensional and multidimensional Fermi surfaces, including two- and three-dimensional sheets. Unfortunately, transport measurements alone cannot separate between these options.

Interestingly enough, similar multidimensional Fermi surface, including two-dimensional (2D) and three-dimensional (3D) sheets, is found in a number of superconductors with rather high transition temperatures. In MgB_2, the anisotropy of electrical resistivity, ρ_c/ρ_{ab}, is about 3.5[31] while 2D and 3D sheets have about the same density of states. In borocarbides, the anisotropy of electrical resistivity is of the order of one[32] while the Fermi surface is composed of both 3D and warped 2D sheets, the latter having well defined nesting areas.[33] In $NbSe_2$ the anisotropy ratio is about 30 (Ref. 34) due to a much larger contributions of the two-dimensional sections of the Fermi surface into transport. In the heavy fermion superconductor $CeCoIn_5$, the anisotropy ratio is small[35] despite the presence of the two-dimensional sheet in the Fermi surface,[36] and is temperature dependent. This temperature-dependent anisotropy reflects the difference in the temperature-dependent resistivity for two current flow directions[37] in $CeCoIn_5$ due to an anisotropy of magnetic scattering.

The superconducting state in all these compounds is anomalous and frequently characterized by strong variation in the superconducting gap magnitude between different

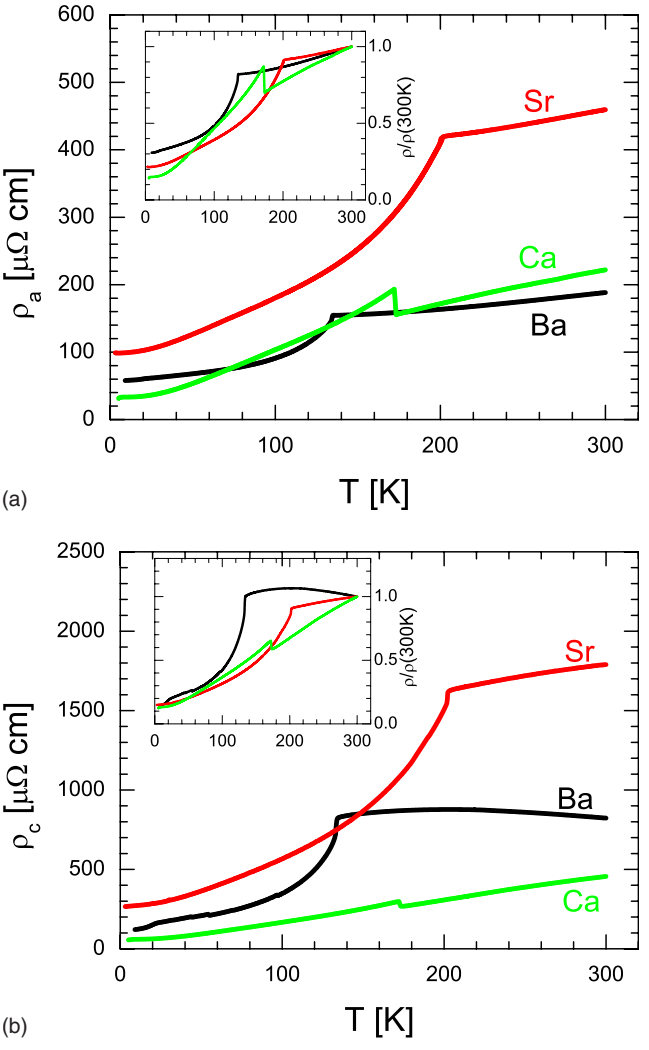

FIG. 12. (Color online) Temperature dependence of the in-plane (top panel) and interplane (bottom panel) resistivity for $CaFe_2As_2$, $SrFe_2As_2$, and $BaFe_2As_2$. The curves were selected as corresponding to a minimum room-temperature resistivity value for each type of the curves. The insets show the same data normalized by the resistivity values at 300 K.

Fermi-surface sheets.[38–41] It is therefore of great interest if it is similar to the case of the iron-arsenic superconductors. Strong temperature dependence of the anisotropy of London penetration depth in optimally doped $Ba(Fe_{1-x}Co_x)_2As_2$ (T_c of 23 K),[15,42] in $(Ba,K)Fe_2As_2$ (T_c of 30 K),[43] and in NdFeAs(O,F),[44] similar to the cases of MgB_2 (Ref. 45) and $NbSe_2$ (Ref. 46), suggests that the situation in iron-arsenic family may be similar.

C. Comparison of the resistivity temperature dependences

In the top panel of Fig. 12 we show temperature-dependent in-plane resistivity of the three compounds; the inset shows the same data normalized by the room-temperature values. Similar plots for the temperature-dependent interplane transport are shown in the bottom panel of Fig. 12.

It is interesting to notice that, despite monotonic change in the anisotropy with the size of the *A* element, resistivity temperature dependences do not show systematic evolution. Moreover, the temperatures of the structural/antiferromagnetic transitions do not follow monotonic trend either, with T_{SM} being maximum for Sr (205 K), followed by Ca (173 K) and Ba (137 K). The in-plane resistivity (top panel of Fig. 12) may be the only other quantity, which follows the same order as T_{SM}, if taking minimum resistivity values. (Strictly speaking, the resistivities of the Ca and Ba compounds at room temperature coincide within the error bars.) This similar trend in the value of the in-plane resistivity and T_{SM} may be suggestive that the proximity to the transition is a factor important for the resistivity. It obviously suggests that pretransition fluctuations play important role in the scattering already at room temperature.

For all three compounds the anisotropy ratio decreases stepwise on passing through T_{SM}. This fact is suggestive that the two-dimensional portions of the Fermi surface, contributing more to the ρ_a, are affected stronger by the transition. This is in line with the idea about possible role of Fermi surface nesting in the transition.

On the other hand, the Ca compound, characterized by the lowest anisotropy, is the only one which clearly shows resistivity increase below the transition for both current flow directions. It also shows notably lower interplane resistivity, and clear metallic character of its resistance temperature dependence both above and below T_{SM}. This clearly suggest that the pretransition fluctuations of the order parameter do not play as large role in the resistivity of the Ca compound as they do in the Ba and Sr compounds.

V. CONCLUSIONS

The parent compounds of iron-arsenic superconductors reveal relatively small anisotropy of the electrical resistivity. The ratio of the interplane and in-plane resistivities stays well below ten for all temperature range studied, and nowhere close to the reported values of about 100.[12–14] The anisotropy increases in line with the ionic radius of *A* element, revealing the same trend as found in band-structure calculations. We do not see any systematic trend in the evolution of the temperature-dependent resistivity (either for the in-plane or interplane) as a function of the size of the alkali earth; neither we see a trend in the variation of the temperature of the sturctural/antiferromagnetic transition. On the other hand, there seems to be a correlation between the value of the in-plane resistivity at room temperature and T_{SM}. We speculate that pretransition fluctuations play important role in scattering.

ACKNOWLEDGMENTS

We thank A. Kaminski and Y. Lee for discussions. M.A.T. acknowledges continuing cross appointment with the Institute of Surface Chemistry, National Ukrainian Academy of Sciences. Work at the Ames Laboratory was supported by the Department of Energy—Basic Energy Sciences under Contract No. DE-AC02-07CH11358. R. P. acknowledges support from Alfred P. Sloan Foundation.

*Corresponding author; tanatar@ameslab.gov
†Permanent address: Materials Science and Technology Division, Oak Ridge National Laboratory, Oak Ridge, TN 37831, USA.
‡Corresponding author; prozorov@ameslab.gov

[1] W. A. Little, Sci. Am. **212**, 21 (1965); Phys. Rev. **134**, A1416 (1964).
[2] V. L. Ginzburg, Zh. Eksp. Teor. Fiz. **47**, 2318 (1964) [Sov. Phys. JETP **20**, 1549 (1965)].
[3] *Problema Vysokotemperaturnoi Sverkhprovodimosti*, edited by V. L. Ginzburg and D. A. Kirzhnits (Nauka, Moscow, 1977) [*High-Temperature Superconductivity* (Consultants Bureau, NewYork, 1982)].
[4] E. Properties, in *Inorganic Quasi-One-Dimensional Compounds, Parts I and II*, edited by P. Monceau (Reidel, Dordrecht, 1985).
[5] T. Ishiguro, K. Yamaji, and G. Saito, *Organic Superconductors*, 2nd ed., Springer Series in Solid State Physics Vol. 88 (Springer, Heidelberg, 1998).
[6] J. G. Bednorz and K. A. Muller, Rev. Mod. Phys. **60**, 585 (1988).
[7] P. C. Canfield and G. W. Crabtree, Phys. Today **56**(3), 34 (2003).
[8] A. P. Mackenzie and Y. Maeno, Rev. Mod. Phys. **75**, 657 (2003).
[9] Y. Kamihara, T. Watanabe, M. Hirano, and H. Hosono, J. Am. Chem. Soc. **130**, 3296 (2008).
[10] M. Rotter, M. Tegel, and D. Johrendt, Phys. Rev. Lett. **101**, 107006 (2008).
[11] S. Lebegue, Phys. Rev. B **75**, 035110 (2007); Fengjie Ma and Zhong-Yi Lu, *ibid.* **78**, 033111 (2008).
[12] X. F. Wang, T. Wu, G. Wu, H. Chen, Y. L. Xie, J. J. Ying, Y. J. Yan, R. H. Liu, and X. H. Chen, Phys. Rev. Lett. **102**, 117005 (2009).
[13] G. F. Chen, Z. Li, J. Dong, G. Li, W. Z. Hu, X. D. Zhang, X. H. Song, P. Zheng, N. L. Wang, and J. L. Luo, Phys. Rev. B **78**, 224512 (2008).
[14] X. F. Wang, T. Wu, G. Wu, R. H. Liu, H. Chen, Y. L. Xie, and X.

H. Chen, New J. Phys. **11**, 045003 (2009).
[15] M. A. Tanatar, N. Ni, C. Martin, R. T. Gordon, H. Kim, V. G. Kogan, G. D. Samolyuk, S. L. Bud'ko, P. C. Canfield, and R. Prozorov, Phys. Rev. B **79**, 094507 (2009).
[16] N. Ni, M. E. Tillman, J.-Q. Yan, A. Kracher, S. T. Hannahs, S. L. Bud'ko, and P. C. Canfield, Phys. Rev. B **78**, 214515 (2008).
[17] N. Ni, S. Nandi, A. Kreyssig, A. I. Goldman, E. D. Mun, S. L. Bud'ko, and P. C. Canfield, Phys. Rev. B **78**, 014523 (2008).
[18] R. Prozorov, N. Ni, M. A. Tanatar, V. G. Kogan, R. T. Gordon, C. Martin, E. C. Blomberg, P. Prommapan, J. Q. Yan, S. L. Bud'ko, and P. C. Canfield, Phys. Rev. B **78**, 224506 (2008).
[19] H. C. Montgomery, J. Appl. Phys. **42**, 2971 (1971).
[20] B. F. Logan, S. O. Rice, and R. F. Wick, J. Appl. Phys. **42**, 2975 (1971).
[21] P. Blaha, K. Schwarz, G. K. H. Madsen, D. Kvasnicka, and J. Luitz, *An Augmented Plane Wave + Local Orbitals Program for Calculating Crystal Properties*, edited by K. Schwarz (TU Wien, Austria, 2001).
[22] J. P. Perdew and Y. Wang, Phys. Rev. B **45**, 13244 (1992).
[23] M. Rotter, M. Tegel, D. Johrendt, I. Schellenberg, W. Hermes, and R. Pottgen, Phys Rev. B **78**, 020503(R) (2008).
[24] M. Tegel, M. Rotter, V. Weiss, F. M. Schappacher, R. Poettgen, and D. Johrendt, J. Phys.: Condens. Matter **20**, 452201 (2008).
[25] A. Kreyssig, M. A. Green, Y. Lee, G. D. Samolyuk, P. Zajdel, J. W. Lynn, S. L. Budko, M. S. Torikachvili, N. Ni, S. Nandi, J. B. Leao, S. J. Poulton, D. N. Argyriou, B. N. Harmon, R. J. McQueeney, P. C. Canfield, and A. I. Goldman, Phys. Rev. B **78**, 184517 (2008).
[26] G. K. H. Madsen and D. J. Singh, Comput. Phys. Commun. **175**, 67 (2006).
[27] S. R. Saha, N. P. Butch, K. Kirshenbaum, and J. Paglione, arXiv:0811.3940 (unpublished).
[28] P. L. Alireza, Y. T. Chris Ko, J. Gillett, C. M. Petrone, J. M. Cole, S. E. Sebastian, and G. G. Lonzarich, J. Phys.: Condens. Matter **21**, 012208 (2008).
[29] D. J. Singh, Phys. Rev. B **78**, 094511 (2008).
[30] I. I. Mazin, M. D. Johannes, L. Boeri, K. Koepernik, and D. J. Singh, Phys. Rev. B **78**, 085104 (2008).
[31] Yu. Eltsev, K. Nakao, S. Lee, T. Masui, N. Chikumoto, S. Tajima, N. Koshizuka, and M. Murakami, Phys. Rev. B **66**, 180504(R) (2002).
[32] I. R. Fisher, J. R. Cooper, and P. C. Canfield, Phys. Rev. B **56**, 10820 (1997).
[33] S. B. Dugdale, M. A. Alam, I. Wilkinson, R. J. Hughes, I. R. Fisher, P. C. Canfield, T. Jarlborg, and G. Santi, Phys. Rev. Lett. **83**, 4824 (1999).
[34] J. Edwards and R. F. Frindt, J. Phys. Chem. Solids **32**, 2217 (1971).
[35] A. Malinowski, M. F. Hundley, C. Capan, F. Ronning, R. Movshovich, N. O. Moreno, J. L. Sarrao, and J. D. Thompson, Phys. Rev. B **72**, 184506 (2005).
[36] R. Settai, H. Shishido, S. Ikeda, Y. Murakawa, M. Nakashima, D. Aoki, Y. Haga, H. Harima, and Y. Onuki, J. Phys.: Condens. Matter **13**, L627 (2001).
[37] M. A. Tanatar, J. Paglione, C. Petrovic, and L. Taillefer, Science **316**, 1320 (2007).
[38] F. Bouquet, Y. Wang, I. Sheikin, T. Plackowski, A. Junod, S. Lee, and S. Tajima, Phys. Rev. Lett. **89**, 257001 (2002).
[39] T. Yokoya, T. Kiss, A. Chainani, S. Shin, M. Nohara, and H. Takagi, Science **294**, 2518 (2001).
[40] E. Boaknin, M. A. Tanatar, J. Paglione, D. G. Hawthorn, F. Ronning, R. W. Hill, M. Sutherland, L. Taillefer, J. Sonier, S. M. Hayden, and J. W. Brill, Phys. Rev. Lett. **90**, 117003 (2003).
[41] M. A. Tanatar, J. Paglione, S. Nakatsuji, D. G. Hawthorn, E. Boaknin, R. W. Hill, F. Ronning, M. Sutherland, L. Taillefer, C. Petrovic, P. C. Canfield, and Z. Fisk, Phys. Rev. Lett. **95**, 067002 (2005).
[42] R. T. Gordon, N. Ni, C. Martin, M. A. Tanatar, M. D. Vannette, H. Kim, G. Samolyuk, J. Schmalian, S. Nandi, A. Kreyssig, A. I. Goldman, J. Q. Yan, S. L. Bud'ko, P. C. Canfield, and R. Prozorov, Phys. Rev. Lett. **102**, 127004 (2009).
[43] C. Martin, R. T. Gordon, M. A. Tanatar, H. Kim, N. Ni, S. L. Bud'ko, P. C. Canfield, H. Luo, H. H. Wen, Z. Wang, A. B. Vorontsov, V. G. Kogan, and R. Prozorov, arXiv:0902.1804 (unpublished).
[44] R. Prozorov, M. A. Tanatar, R. T. Gordon, C. Martin, H. Kim, V. G. Kogan, N. Ni, M. E. Tillman, S. L. Bud'ko, and P. C. Canfield, arXiv:0901.3698 (unpublished).
[45] J. D. Fletcher, A. Carrington, O. J. Taylor, S. M. Kazakov, and J. Karpinski, Phys. Rev. Lett. **95**, 097005 (2005).
[46] J. D. Fletcher, A. Carrington, P. Diener, P. Rodiere, J. P. Brison, R. Prozorov, T. Olheiser, and R. W. Giannetta, Phys. Rev. Lett. **98**, 057003 (2007).